The Fractal Dimension correlated to the bone mineral density

Khaled HARRAR[1], Latifa HAMAMI[2]

Ecole Nationale Polytechnique, Département d'Electronique, Laboratoire Signal et communications,
BP 182 El-Harrach 16200 Alger ALGERIE,
[1]hk_robot@yahoo.fr, [2]latifa.hamami@enp.edu.dz

Abstract: - Osteoporosis is a condition of decreased bone mass. This leads to fragile bones which are at an increased risk for fractures, more often, it affects postmenopausal women. In this paper we propose a study of osteoporosis with the fractal dimension. After an introduction to the theory and fractal dimension, we use the box counting method for the segmentation of radiographic images, the study of the influence of range size boxes on the fractal dimension will be investigated, and the correlation between a reference dimension and bone mineral density. Other imaging techniques will be given in order to see the results of the application of the method on these types of images.

Key-Words: - Box counting method, Osteoporosis, Fractal dimension, Radiographic images, Side length, Threshold.

1 Introduction

A fractal is generally "a rough or fragmented geometric shape that can be subdivided into parts, each of which is (at least approximately) a reduced size copy of the whole," a property called self-similarity [1]. The term was coined by Benoît Mandelbrot in 1975 and was derived from the Latin *fractus* meaning "broken" or "fractured." A fractal often has the following features:

- It has a fine structure at arbitrarily small scales.
- It is too irregular to be easily described in traditional Euclidean geometric language.
- It is self-similar (at least approximately or stochastically).
- It has a Hausdorff dimension which is greater than its topological dimension (although this requirement is not met by space-filling curves such as the Hilbert curve).
- It has a simple and recursive definition [2].

Because they appear similar at all levels of magnification, fractals are often considered to be infinitely complex (in informal terms). Natural objects that approximate fractals to a degree include clouds, mountain ranges, lightning bolts, coastlines, and snow flakes. However, not all self-similar objects are fractals—for example; the real line (a straight Euclidean line) is formally self-similar but fails to have other fractal characteristics. In this paper we use the fractal dimension as tool to study the osteoporosis which is a disease of bone leading to an increased risk of fracture. In osteoporosis the bone mineral density (BMD) is reduced, bone microarchitecture is disrupted, and the amount and variety of non-collagenous proteins in bone is altered. Osteoporosis is defined by the World Health Organization (WHO) in women as a bone mineral density 2.5 standard deviations below peak bone mass (20-year-old sex-matched healthy person average) as measured by DXA; the term "established osteoporosis" includes the presence of a fragility fracture. To reduce the enormous costs associated with osteoporotic fractures, diagnostic techniques have to be optimized. The most widely used diagnostic technique in assessing osteoporosis is bone mineral densitometry with either dual-energy X-ray absorptiometry (DXA) which measures areal density of the spine, hip and radius or quantitative computed tomography (QCT) which measures volumetric density of the spine, are routine diagnostic procedures for assessing and monitoring osteoporotic changes; These methods are accurate in determining bone mass, which has been shown to be a good predictor of fracture risk in osteoporosis. There is, however, a considerable overlap of bone mineral density (BMD) measurements for patients with osteoporosis and healthy subjects without fracture risk. Studies have indicated that the BMD alone may be insufficient to determine the strength of cancellous bone, and that the trabecular architecture is an important factor in

assessing bone strength [3]. Several imaging techniques have been described to examine trabecular bone structure, such as projectional radiography, high-resolution CT (HRCT) and high-resolution MRI (HRMRI). Image and structure analysis schemes have been adapted to the individual imaging modalities. Recently, ultrasound has been established as a technique that assesses bone structure in addition to BMD. The fractal dimension is a powerful tool to detect and study the osteoporosis for all techniques of imaging, for this goal the box counting method is used. We have developed a new methodology based on fractal analysis of radiographic images. Our approach exploits a model reference bone. A fractal dimension with the box-counting method is used to estimate the osteoporosis. The fractal dimension of a reference bone model is calculated, where the image is taken from DXA technique. When a patient suffers from a pathology, an X-ray image is taken and the fractal dimension of this image is estimated, finally it's compared to the fractal dimension of that calculated in the reference image (reference bone model), that leads us to conclude there is a correlation between the assessment of BMD and the fractal dimension.

2 Material and methods

2.1 Diagnostic of osteoporosis

The diagnosis of osteoporosis is made on measuring the bone mineral density (BMD). The most popular method is dual energy X-ray absorptiometry (DXA or DEXA). In addition to the detection of abnormal BMD, the diagnosis of osteoporosis requires investigations into potentially modifiable underlying causes; this may be done with blood tests and X-rays. Depending on the likelihood of an underlying problem, investigations for cancer with metastasis to the bone, multiple myeloma, Cushing's disease and other above mentioned causes may be performed. Dual energy X-ray absorptiometry (DXA, formerly DEXA) is considered the gold standard for the diagnosis of osteoporosis. Osteoporosis is diagnosed when the bone mineral density is less than or equal to 2.5 standard deviations below that of a young adult reference population. This is translated as a T-score. The World Health Organization has established the following diagnostic guidelines [1][4]:

- T-score -1.0 or greater is "normal"

- T-score between -1.0 and -2.5 is "low bone mass" (or "osteopenia")
- T-score -2.5 or below is osteoporosis

When there has also been an osteoporotic fracture (also termed "low trauma-fracture" or "fragility fracture"), defined as one that occurs as a result of a fall from a standing height, the term "severe or established" osteoporosis is used.

2.2 State of art

Authors have published methods, one can cite for instance:

-The texture analysis of proximal femur radiographs for osteoporosis assessment, Gabor filter is used to calculate features from trabecular pattern recorded on radiographs of proximal femur [5]. The extracted features represent the quality or structure of the bone, better quality represents better bone strength, lower quality leads to low bone strength and could be suspected as osteoporosis. Extracted features from trabecular pattern recorded in proximal femur radiographs by Gabor filter match with their predetermined Singh index.

- A morphometric analysis system of digital radiographic images was constructed for the clinical evaluation of bone trabecular structural change [6]. This system consisted of computed radiography, a mathematical morphological filter, skeletal morphometric measurements, star volume analysis, and node-strut analysis. The computed radiographic data were morphologically processed, and the trabecular structure was extracted as binary skeletal images. Analyses were made with regard to the skeletal number, separation, perimeter, complexity, continuity, and connectivity. A trial study of this system was used to evaluate the therapeutic efficacy of vitamin K2 in the osteoporotic patients.

- Another method can indicate a correlation between bone mass density and 2nd harmonic ultrasound generation [7]. In addition to the 2nd harmonic amplitude variation with the degree of the disease, there is a similar variation of the duration of this signal. A numerical estimation of this variation is proposed.

- Lacunarity analysis has been used to determine relevant parameters to differentiate among three types of trabecular bone structure (healthy young, healthy perimenopaused, and osteoporotic patients) from lumbar vertebra MR images [8].

2.3 Image Acquisition

Since fractal dimension is a powerful yet simple tool and is widely used for analysis of the trabecular bone structure for all image techniques, we have taken the conventional radiography for its economical advantages. X-ray images of forearm distal bone were taken for a group of 50 subjects of different age. The same persons were measured the forearm bone mineral density using dual-energy X-ray absorptiometry. The X-ray images were all taken at 53 kV and 4 mAs, and films were developed using the same chemical process. A calibration phantom Agfa Mamoray of specified absorption of X-ray radiation was placed in each image. The images were digitized at 7 bit/pixel using a CCD camera. The digital images were brightness-standardized by making the phantom average brightness the same in all images. A 256x256-pixel region of interest (ROI) was defined in the field of every image, as shown in Figure 1[9].

Fig. 1. Example of an X-ray image of distal forearm bone with a square ROI.

3. Image preprocessing

3.1 Thresholding by histogram

Before image processing, we prepare the image for better quality, for this reason we have to apply a thresholding to the image. There are lots of methods to choose the threshold; in this section we present it by using a histogram (Fig 2), in this case the threshold was chosen by calculating the average on the histogram; this is an important tool in image processing and is widely used [10].
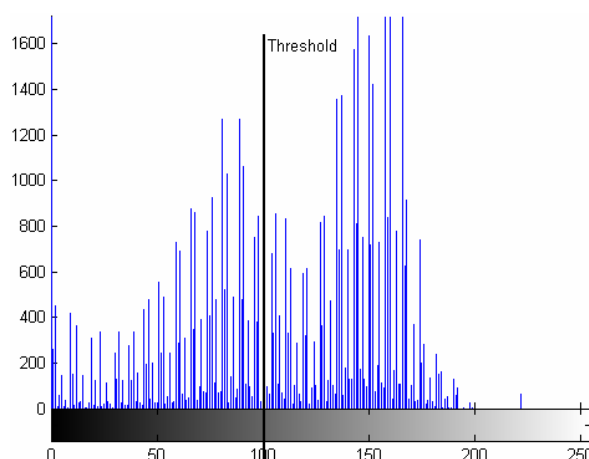

Fig. 2. Histogram of the image of the figure. 1

3.2 Filtering the image

In Signal processing or image processing it is usually necessary to use filters [11][12][13]. To obtain the best image quality, it is vital to perform a high level noise reduction before performing the image processing steps. Always in the way to get a good quality of the image it's necessary to perform high degree of noise reduction in an image before performing higher-level processing steps. The median filter is a non-linear digital filtering technique, often used to remove noise from images. The idea is to examine a sample of the input and decide if it is representative of the signal. This is performed using a window consisting of an odd number of samples. The values in the window are sorted into numerical order; the median value, the sample in the center of the window, is selected as the output. The oldest sample is discarded, a new sample acquired, and the calculation repeats.

4. Image processing

4.1 The dimension and fractals

A known method to measure a length, surface or a volume consists in covering sets with paving stones (then its only a question of counting the number of paving stones to obtain the length, surface or volume of the set), of which the length, surface or volume is taken as measuring unit. If ε is the side (length standard) of a paving stone, measurement obtained is [14]:

$$M = N . \varepsilon^{d} = N \mu \qquad (1)$$

Where μ is the unit of measure (length, surface or volume). Mandelbrot postulates that there are curves of intermediate size between 1 and 2 of surfaces of size higher than 2, and that these objects precisely have the property to have no length or a precise surface, not more than one volume does not have a surface or a square does not have a length. This dimension, intermediary between the integer values, was baptized neologism "fractal" so that no confusion is made between a traditional surface (of D = 2 dimension) [15]. One is brought to believe that a geometrical object, about scale, can also generate as well the small as the big details. Such an object will be known as to have an internal homothety, or to be self-similar. It is known that if one transforms a line by a homothety of arbitrary ratio, whose centre belongs to it, one finds this same line, and it is the same for any plane and entire Euclidean space. In fractal geometry, the fractal dimension, D, is a statistical quantity that gives an indication of how completely a fractal appears to fill space, as one zooms down to finer and finer scales. There are many specific definitions of fractal dimension and none of them should be treated as the universal one. From the theoretical point of view the most important are the Hausdorff dimension, the packing dimension and, more generally, the Rényi dimensions. On the other hand the box-counting dimension and correlation dimension are widely used in practice, partly due to their ease of implementation. Although for some classical fractals all these dimensions do coincide, in general they are not equivalent. For example, what is the dimension of the Koch snowflake? It has topological dimension one, but it is by no means a curve-- the length of the curve between any two points on it is infinite. No small piece of it is line-like, but neither is it like a piece of the plane or any other. In some sense, we could say that it is too big to be thought of as a one-dimensional object, but too thin to be a two-dimensional object, leading to the question of whether its dimension might best be described in some sense by number between one and two. This is just one simple way of motivating the idea of fractal dimension. There are two main approaches to generate a fractal structure. One is growing from a unit object, and the other is to construct the subsequent divisions of an original structure, like the Sierpinski triangle (Fig. 3) [2]. Here we follow the second approach to define the dimension of fractal structures. If we take an object with linear size equal to r residing in Euclidean dimension, and reduce its linear size to be r in each spatial direction, it takes $N(r)$ number of self similar

objects to cover the original object. However, the dimension defined by:

$$D = \frac{\log N(r)}{\log \frac{1}{r}} \qquad (2)$$

is still equal to its topological or Euclidean dimension [1]. By applying the above equation to fractal structure, we can get the dimension of fractal structure (which is more or less the Hausdorff dimension) as a non-whole number as expected.

$$D = \lim_{\epsilon \to 0} \frac{\log N(\epsilon)}{\log \frac{1}{\epsilon}} \qquad (3)$$

where $N(\epsilon)$ is the number of self-similar structures of linear size ε needed to cover the whole structure. For instance, the fractal dimension of Sierpinski triangle (Fig.3) is given by:

$$D = \lim_{\epsilon \to 0} \frac{\log N(\epsilon)}{\log \frac{1}{\epsilon}} \qquad (4)$$

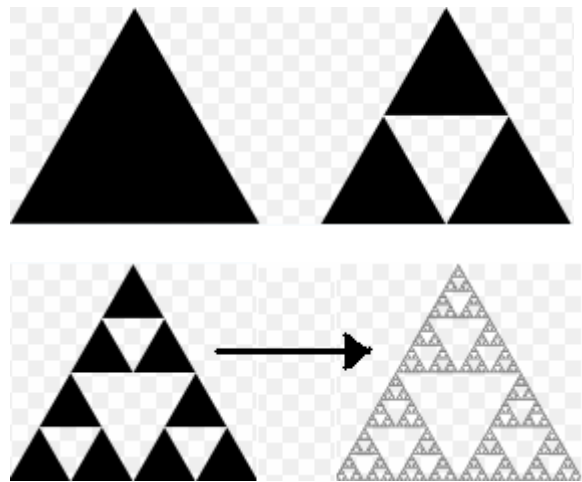$$= \lim_{k \to \infty} \frac{\log 3^k}{\log 2^k} = \frac{\log 3}{\log 2} \approx 1.585$$

Fig. 3. Sierpinski triangle

Closely related to this is the box-counting dimension, which considers, if the space were divided up into a grid of boxes of size ε, how does the number of boxes scale that would contain part of the attractor? Again:

$$D_0 = \lim_{\epsilon \to 0} \frac{\log N(\epsilon)}{\log \frac{1}{\epsilon}} \qquad (5)$$

Other dimension quantities include the information dimension, which considers how the average information needed to identify an occupied box scales, as the scale of boxes gets smaller:

$$D_1 = \lim_{\epsilon \to 0} \frac{-\langle \log p_\epsilon \rangle}{\log \frac{1}{\epsilon}} \qquad (6)$$

and the correlation dimension, which is perhaps easiest to calculate,

$$D_2 = \lim_{\epsilon \to 0, M \to \infty} \frac{\log(g_\epsilon / M^2)}{\log \epsilon} \qquad (7)$$

where M is the number of points used to generate a representation of the fractal or attractor, and g_ϵ is the number of pairs of points closer than ε to each other. It should be checked that the curves do not have double points. It is not the same with other curves which have a double infinity of points. It follows that for them, the concept of paving changes significance and that the definition of the homothety dimension becomes debatable.

4.2 The box counting method

Linear fractal images are the outcome of absolute generating processes and the information related to each step of the process can be calculated exactly [16][17]. For instance, in a linear fractal image like Koch boxes, seven new segments, three times smaller than the previous segment, are generated at each step in the generating process. Therefore, an exact mathematical calculation procedure follows. After the first step, the image contains seven segments whose size is 1/3 that of the initial value; after the second step, the image contains 49 segments of size 1/9; and so on. In linear fractals, even after two steps of the generating process, the fractal dimension can be calculated exactly. In non-linear fractal images, because of the existence of random elements there is a statistical (i.e., not deterministically mathematical) generating process and the information available at each step of the generating process is not exact [15][17]. Natural fractals fall into this category of fractals. For this reason, an appropriate method is needed to estimate the fractal dimension of non-linear images. Among

the techniques discussed by Mandelbrot, the box counting method is found like the most adapted for the estimate of fractal dimension [1][18]. Voss, Keller and Sarkar carried out a box counting method, the purpose of which is to consider the average number, noted N (r), of cubic boxes with fixed side length r, necessary to cover the image, considered as a surface in R^3 space [19][20][21]. For that we estimates P (m, r), the probability that one box of size r, centered on an arbitrary point of surface, contains m points of the set. We have thus [22]:

$$\forall r, \sum_{m=1}^{Np} P(m,r) = 1 \qquad (8)$$

Where, Np is the number of possible points in the cube. The estimate of the average number of disjoined boxes necessary to cover surface is :

$$N(r) = \sum_{m=1}^{Np} N(m,r) = \sum_{m=1}^{Np} \frac{P(m,r)}{m} \qquad (9)$$

The estimate by the least squares method of the slope of the group of dots (log (r), - log (N (r))), obtained with boxes of increasing size r, and gives the estimate of fractal dimension. The algorithm 1 presents this calculation [16]:

```
Initialization:
FOR r =1 to r_max and m = 1 to r^3 DO
        P(m,r) = 0
FOR any site s of the image DO
        BEGIN
        For r = 1 to r_max DO
                BEGIN
                  - Center a cube with
                    dimension r on [s, A[s]]
                  - Count the number m of
                    pixels of the image
                    which belong to this cube
                  - Increment P (m,r) by 1
                END
        END
FOR  r = 1 to r_max DO
```
$$N(r) = \sum_{m=1}^{Np} \frac{P(m,r)}{m}$$
```
Estimate by the method of least squares the slope D
of the curve (log (r), -log (N(r)) )
```

Algorithm. 1. The box counting method algorithm.

The mathematical method (box counting method) is illustrated in the algorithm 1 for any image of

dimension 3. After the application of the threshold and the filter of the image, one initializes the probability to find a box of the side length 'r' and contains m pixels to 0. After that, for any pixel 's' of the image, we centre a cube (box) with dimension 'r', as a result one counts the number 'm' of pixels which belong to this box and increments the probability $P(m,r)$ by 1 , i.e. if a box containing $m \neq 0$ is found, the number of boxes is incremented. We repeat this operation from $r = 1$ to r_{max} (chosen), after that for each r, we calculate $N(r) = sum(P(m,r) / m)$. Finally by the method of least square we calculate the slope 'D' which is the fractal dimension of the curve $(\log (r), -\log(N(r)))$.

We can explain this method as follow:

We apply a grid on the image where the side length of the boxes $= r$, for each operation (fig .4), we calculate 'm' pixels belonging to each box, then we increment $P(m,r)$ if $m \neq 0$. Finally, we calculate $N(r)$ for each grid, which will result in $r = 1$ up to r_{max} (chosen) $N(r) = sum (P (m,r) / m)$; therefore, to calculate the fractal dimension D, we use the definition, i.e. The slope of the curve $(\log (r), -\log(N(r)))$.
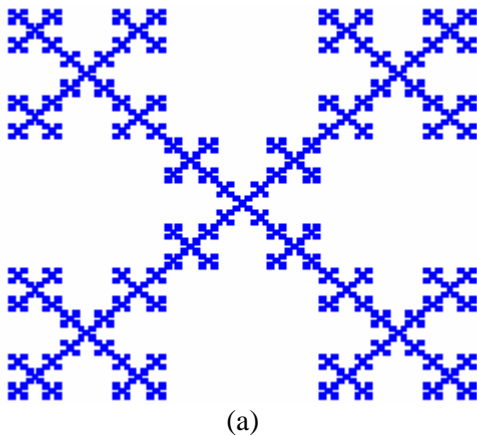
(a)
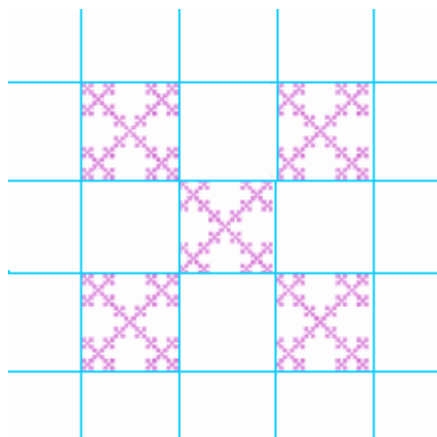
(b)
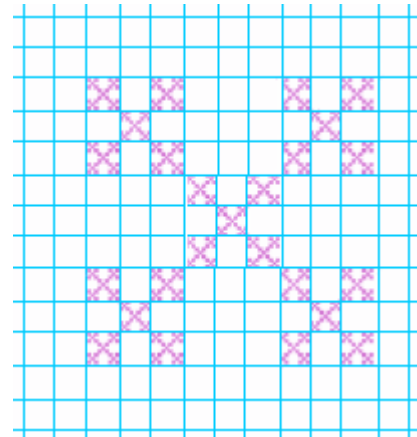
(c)

Fig. 4. Example of calculate the fractal dimension of the Box Fractal.

This is an example of using box-counting method; we put the fractal on a sheet of graph paper (grid). For this fractal, we use boxes with sizes 1/3 and 1/9. In the first case, 5 boxes are not empty. In the second case, there are 25 boxes and in the third there are 125. Using these numbers, we find that in the first case D = log 5 / log [1/(1/3)] = 1.46. If you do it for the second case, you will find that the answer is the same, which means that our dimension is accurate.
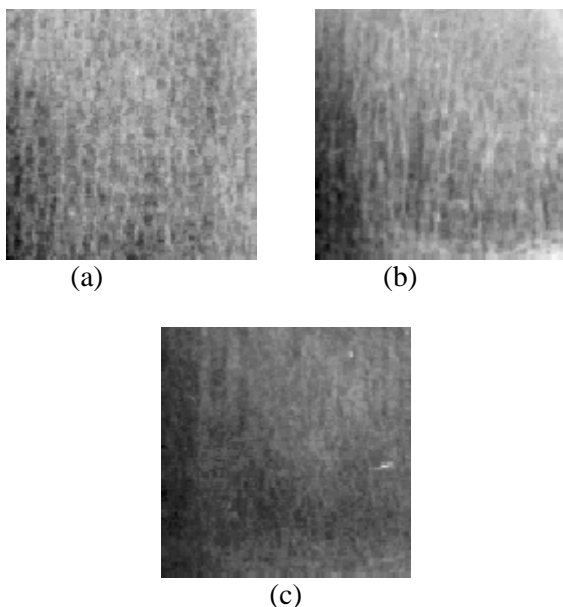
5. Result

Before using the Box counting method in radiographic images of patients who are suffering from the disease, we have to estimate the fractal dimension of a reference or an ideal bone. The concept to find the fractal dimension using the box counting method in radiographic images is not simple, and the assessment of BMD with this dimension is complex because many factors could affect the calculation/results (region imaging, side length box, r_{min} and r_{max},……). To compare the fractal dimension of a radiographic image with that of the reference model, we take a radiographic image of a healthy bone, or an artificial bone similar to the technique in absorptiometry, (so-called reference or ideal bone model), we calculate its fractal dimension, and the corresponding BMD is known (T-score). When a patient is present for the estimation of a BMD, a radiographic image is made and the new fractal dimension is calculated. The bigger fractal dimension is, or the bigger the gap between the patient's fractal dimension and the reference fractal the higher the severity of the disease. Altogether, 50 X-ray bone images were

digitally recorded. The images represented forearm bones of different BMD level that was independently measured for each subject by means of the DXA technique. Based on the densitometry results, the whole group of subjects was divided into 3 categories:
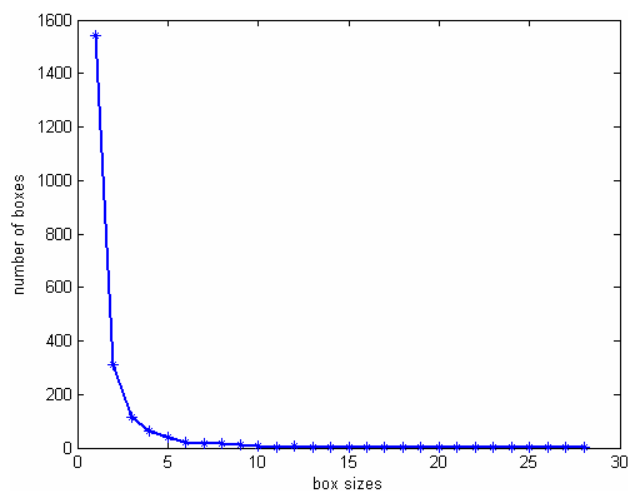
Normal (16 subjects), of physiological loss of calcium (beginning osteoporosis or osteopenia, 16 subjects), and of abnormal loss of calcium, i.e. severe osteoporosis (18 subjects). For every texture parameter, its mean and standard deviation were computed within each of the three groups of patients (Table 1).

Table 1. T-score – result of DXA examination (difference to population BMD mean of young people, normalized to standard deviation), $\mu(\sigma)$ - mean value (standard deviation) of a given parameter.
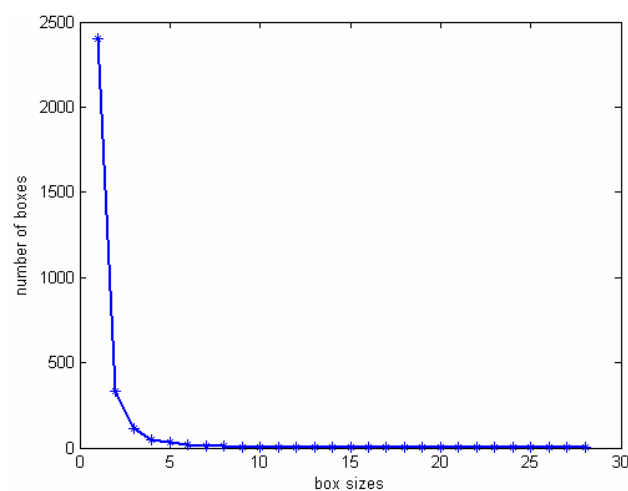
# subjects	T-score		BMD g/cm$_2$
16	Sd > -1	μ	0,50
		σ	0,2
16	-1$\geq$ Sd < -2.5	μ	0,35
		σ	0.06
18	Sd $\leq$ -2.5	μ	0,14
		σ	0.11

(a)   (b)

(c)

Fig. 5. Sample X-ray images of bone tissue for different BMD coefficients (a) BMD = 0.50 g/cm2, (b) BMD = 0.35 g/cm2, (c) BMD = 0.14 g/cm2.

In what follows we will apply the method for the images X-ray test (Fig. 5) of size 125x125 pixels in grayscale, and see the results of the calculation of fractal dimension. For that, we propose to plot curves giving the number of boxes versus their side length r, then the straight regression line which estimates as well as possible the log (N(r)) versus log (1/r); the plot will be done on all the points and outdistances it between the size of boxes is equal to 1.
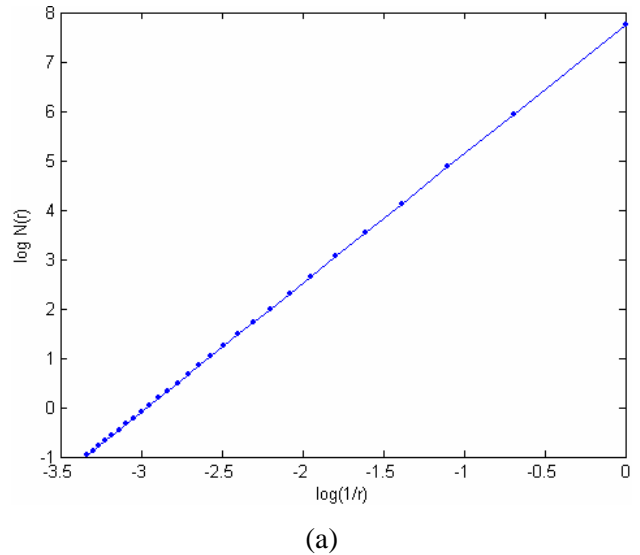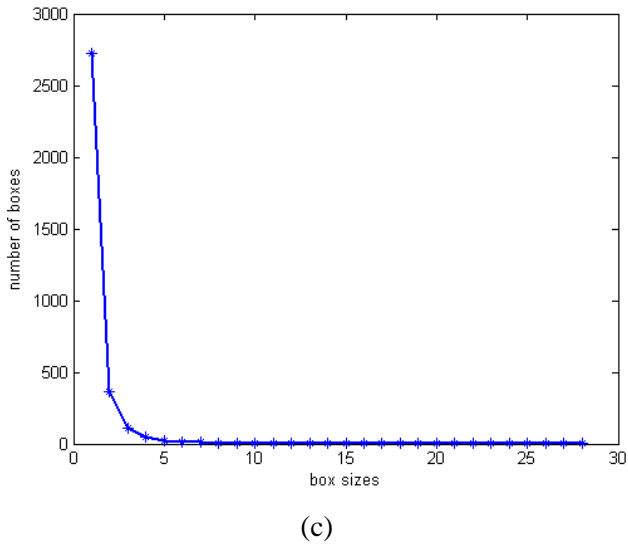

(a)

(b)

(c)

Fig. 6. The plot of the number of boxes versus the side length r for the figure 5, (a) BMD = 0.50 g/cm2, (b) BMD = 0.35 g/cm2, (c) BMD = 0.14 g/cm2.

The Figure 6 represents the number of boxes according to their sizes (r), in this case r = 1 to 28. We notice that the smaller the r the more the number of boxes, and inversely, the more we increase r the smaller the number of boxes. In addition we see a sharp fall of number of boxes after length r = 1, this explains the existence of a significant number of boxes if we fix the side length r at 1. When r reaches 20 or beyond, it becomes increasingly challenging to count the number of boxes, for this we give a table of some values to see what happens for boxes which side length r = 1 to 28 (Table 2).
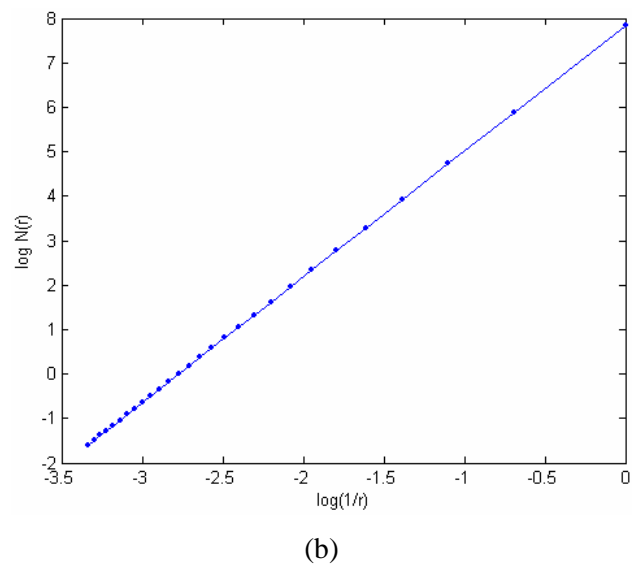
Table 2. Some values of a number of boxes according to the side length r.

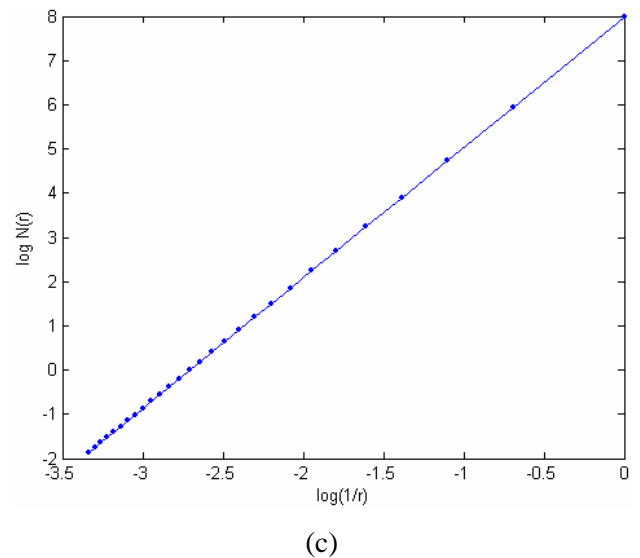| r	N(r) Fig. 6(a)	N(r) Fig. 6(b)	N(r) Fig. 6(c)
1	1540	2402	2727
2	312	115	362
3	116	115	109
4	64	50	44
5	39	31	25
6	24	16	17
7	15	13	10
8	11	9	7
9	11	7	6
10	7	5	4
15	3	3	3
20	2	2	2
25	1	1	1
28	1	1	1

(a)

(b)

(c)

Fig. 7. The plot regression of the curve log N(r) versus log (1/r) by the method of least squares, (a) BMD = 0.50 g/cm2, (b) BMD = 0.35 g/cm2, (b) BMD = 0.14 g/cm2.

In this experiment we obtained a dimension $Da = 2.61$ applied to the figure 5 (a), $Db = 2.83$ applied to the figure 5 (b), and $Dc = 2.95$ applied to the figure 5 (c), for $r = 1$ to 28 according to their BMD. The only parameter which can influence the calculation of fractal dimension is the actual range of the sizes of the windows (boxes). This point will be expanded in the next section.

5.1 The range of box sizes

In using the box-counting method, challenges arise when the range of box sizes is to be determined. In particular, defining the largest and smallest box sizes to use requires extreme care. In addition, the positioning of the grid to superimpose on the image has a critical effect on resulting estimate of fractal dimension. Therefore, both factors should be verified [23][24]. To find fractal dimension, it is challenging to choose the sizes of the boxes for complex images, like the radiographic images. Several tests were carried out on different sizes and the values of fractal dimension were obtained.
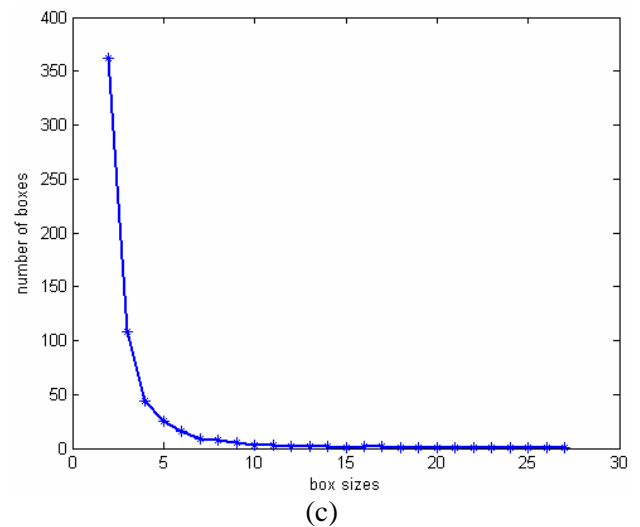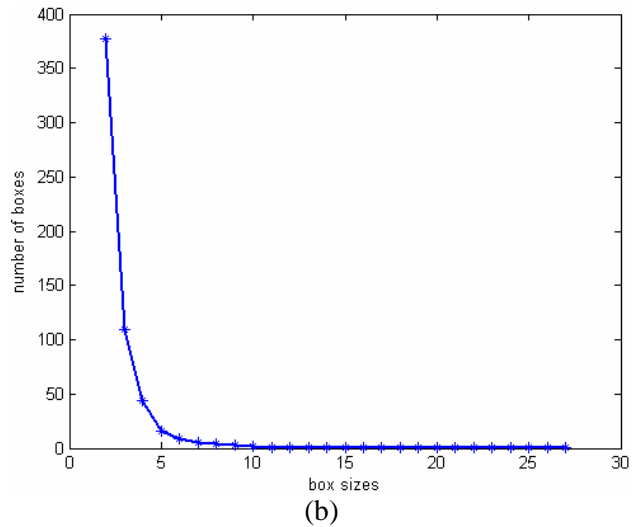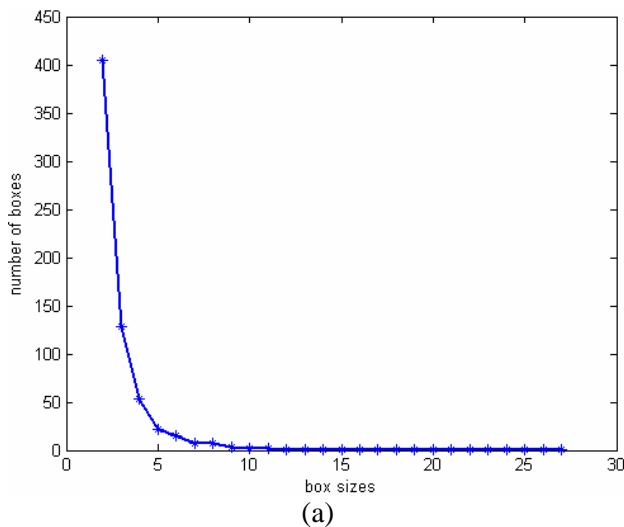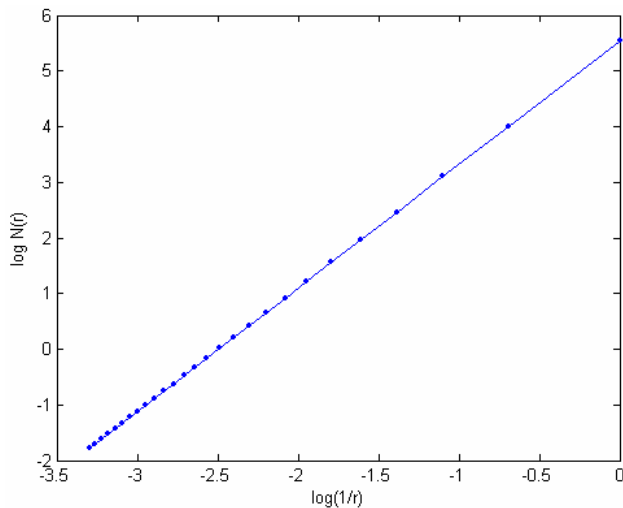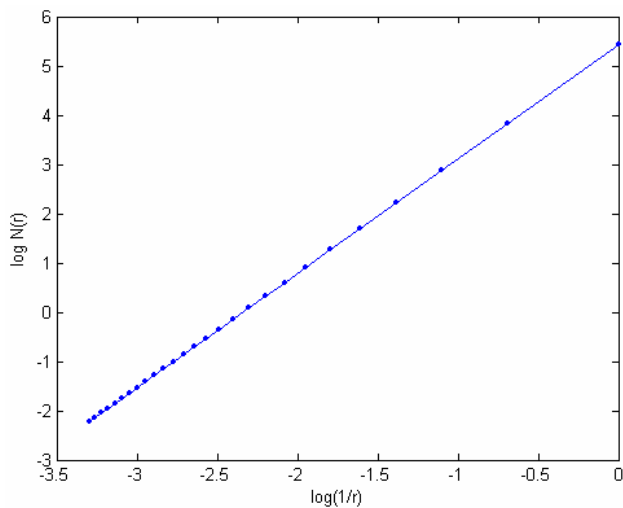
(a)

(b)

(c)

Fig. 8. The box counting method with $r_{min} = 2$, $r_{max} = 27$, applied to the image of figure 5, (a) BMD = 0.50 g/cm2, (b) BMD = 0.35 g/cm2, (c) BMD = 0.14 g/cm2.
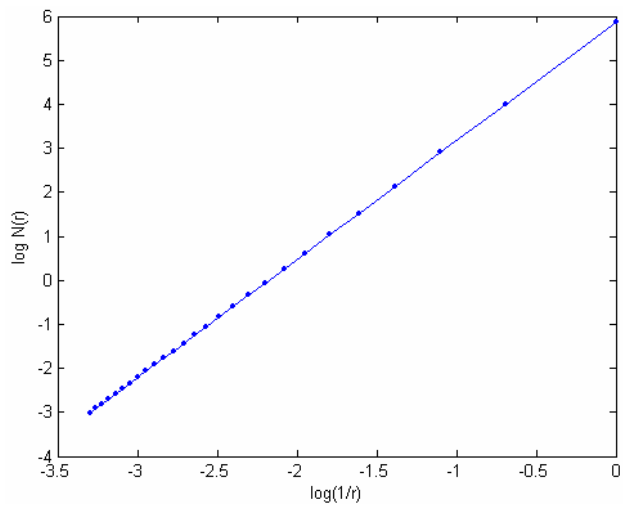
The change in range is illustrated in figure 8, and we notice that the number of boxes change.

(a)

(b)

(c)

Fig. 9. The regression of the curve log N(r) by the least squares method, (a) BMD = 0.50 g/cm2, (b) BMD = 0.35 g/cm2, (c) BMD = 0.14 g/cm2.

The change in range resulted different results for the same images compared to the previous range, the fractal dimensions in this case are: Da = 2.22, Db = 2.32, Dc = 2.39 and this for r_{min} = 2 and r_{max} = 27, Therefore we can conclude that there are 4 possibilities:

- r_{min} small, r_{max} small
- r_{min} small, r_{max} large
- r_{min} large, r_{max} small
- r_{min} large, r_{max} large

Of course it is necessary that they are sufficiently isolated to avoid the effect of overlapping. We give in table 3 certain values of fractal dimension corresponding to the range of the box sizes. This last informs us about the influence of range of the box size on the calculation of fractal dimension.

Table 3. Some examples of the fractal dimension.

r_{min} - r_{max}	Da (BMD = 0.50 g/cm2)	Db (BMD = 0.35 g/cm2)	Db (BMD = 0.14 g/cm2)
1 – 28	2.61	2.83	2.95
1 – 27	2.63	2.91	2.94
2 – 27	2.22	2.32	2.39
2 – 28	1.68	1.85	1.96
1 – 25	2.56	2.69	2.92
2 – 25	1.54	1.65	1.82

5.2 Choice of box sizes

If we see table 3, we notice a variability of values for the fractal dimension, an improvement of the original method can be implemented, it is the choice of r_{min} and r_{max} [25]. Up to now it is difficult to choose the side length r of the boxes considering the complexity of the images, but we can always compromise between r_{min} and r_{max}, these two parameters are not only influential to one another, but more importantly on the calculation of the fractal dimension. For the choice of r_{min} and after several tests carried out, it is safe to say that we can choose r from 2; this will give us a greater probability of finding at least one box; so, for r_{min} = 1, we are confronted with the problem of the pixel size, where a 1x1 box cannot be centered due to its single pixel point. The isolated pixels at r_{min} = 1 should not be taken into consideration, so r_{min} = 2, is a good choice to find a box and to detect pixels going up to 4 (2x2). For r_{max}, it is fixed in the following way:

As soon as N(r) get too close or overlap each other, we stop the process; from there, an extraction of the maximum value of r is carried out. We can also fix

it from the moment when the number of windows (boxes) decreases towards zero (this number must stop at 1); from this moment it is not necessary to repeat the iterations for larger sizes. In addition, the value of r_{max} should not exceed the framework of the image, where:

- If the horizontal size of the image (x) $\leq$ to the vertical size of the image : $r_{max} < x/2$.
- If the vertical size of the image (y) $\leq$ to the horizontal size of the image : $r_{max} < y/2$.

6. Discussion

The fractal dimension reflects roughness of the bone image texture that is related to the bone microarchitecture (Table 4). It is of high importance, because mechanical endurance of the bone tissue depends largely on the state of the bone internal structure. For a subject suffering from osteoporosis (BMD = 0.14 g/cm2, T-score = -6.63), the fractal dimension (Db = 2.95). As seen in Table 3, the values of fractal dimension are lower for healthy subjects in this study. Image brightness shows the highest correlation to BMD. This can be explained by the fact that lower calcium contents results in lower attenuation of X-rays in the bone, so the photographic film becomes darker and digital image brightness is reduced. This applies to brightness-equalized images. It is evident that image brightness standardization is a necessary preprocessing step for reliable analysis of the study of the mineral bone density. We have seen in the previous section that the choice of range of r affected the measure of the fractal dimension in the radiographic images; the same problem is located in the images of the ideal bone model or reference bone model. So for instance we choose a box range (from r_{min} to r_{max}) as an example, and see the correlation between the BMD and both of the fractal dimensions (reference image and image of a patient respectively). We know that the fractal dimension of an ideal bone is very low, because its' microarchitecture density is very high.

Table 4. Correlation the both fractal dimension with BMD.

patients	T-score	BMD	r_{min}-r_{max}	D	D_{ref}
16	Sd > -1	0,50	1 - 28	2.61	2.0
16	-1≥Sd<-2.5	0,35	1- 28	2.83	2.0
18	Sd ≤-2.5	0,14	1 - 28	2.95	2.0

As discussed previously, the reference fractal dimension is known by its calculation, in reference of the radiographic image of healthy subject, or an ideal bone. If we take D_{ref} = 2.0 as an example, we can see the difference between the fractal dimensions in the ROI at different ages. We know by definition the higher the fractal dimension the more the osteoporosis increase. If we look at table 4, this definition is verified: for BMD = 0.50 g/cm2, the fractal dimension = 2.61, for BMD = 0.35 g/cm2, this fractal dimension = 2.83 and it's equal to 2.95 for BMD = 0.14 g/cm2, so there is a correlation between the fractal dimension and the BMD (Fig. 10). An alternative way to confirm the disease is to do a simple arithmetic operation:

Final fractal dimension = D - D_{ref}

We calculate this final fractal dimension and we compare it with the others, for BMD = 0.50 g/cm2, final fractal dimension = 0.61 and for BMD = 0.14 g/cm2, final fractal dimension = 0.95; 0.61 < 0.95, thus we can conclude in this case, the osteoporosis is severe, i.e. the subjects with BMD of 0,50 g/cm2 are more healthier than those with BMD of 0.14 g/cm2 because their fractal dimension is closer to the reference fractal dimension than the other one.
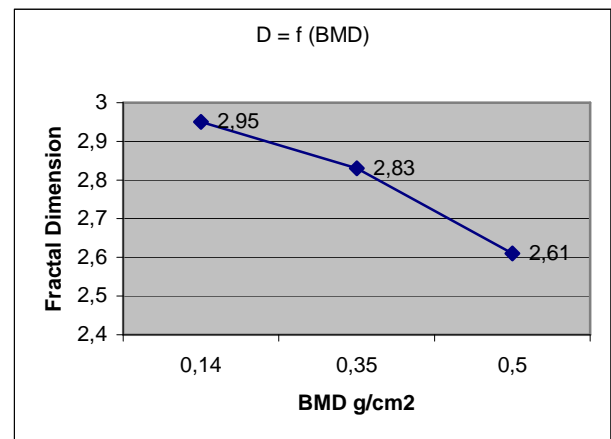

Fig 10. The Fractal Dimension correlated to the bone mineral density.

One can conclude that by measuring changes in fractal dimensions parameters of X-ray images it is possible to monitor changes in calcium contents and internal structure of the bone. Fractal dimension by the box-counting method analysis shows potential usefulness as an aid to the diagnosis of skeletal diseases. Recent studies on the fractal dimension using the box counting method in the radiographic images were made, which have conducted a fractal analysis (with the box-counting method for a binary images) of low-dose digital chest phantom radiographs and calculate fractal-feature distance using the fractal dimension. This method uses more

resources than the method offered [26]. Several methods of fractal mathematics have been applied for analysis of cancellous bone [27][28][29][30]. These include a surface area technique, a boundary tracking algorithm combined with box counting dimension, In those studies, a certain discrimination of the degree of osteoporosis was possible [27][28][30]. The calculation of the fractal dimension in dependency of the binarization threshold value further improves the classification, in our method we calculate the threshold by histogram, and it differs from an image to another, this method calculates the best threshold for the image in the preprocessing step. Also in other studies using box counting methods, the influence of the side length has never been carried out, in our case we have shown that the range of the side length influence the calculation of the fractal dimension and how to choose this parameter [31][32][33][34][35]. The originality of our method is the use of the reference fractal dimension, and the correlation with the BMD, we have optimized our method in all points of view, i.e. its ease of implementation and economical properties, yet keeping the powerful tool to study the disease.

7. Some Examples

In this section we would like to present some other techniques of imaging and apply our method to study osteoporosis. Imaging techniques have been used at different skeletal sites: (a) conventional radiography at the calcaneus, the distal radius, the phalanges, the spine and the femur [36][37][38][39]; (b) magnification radiography at the spine [40]; (c) high-resolution CT at the spine [41]; and (d) high-resolution MRI at the calcaneus (Table 5) [42].

7.1 Magnification radiography

Magnification radiography is a radiography using a micro focal X tube and increased subject-film distance to provide geometric magnification of the subject without unacceptable loss of sharpness and resolution or an undesirable increase in radiation exposure caused by increasing the distance between the subject and the film.

Table 5. Imaging techniques used at different skeletal sites

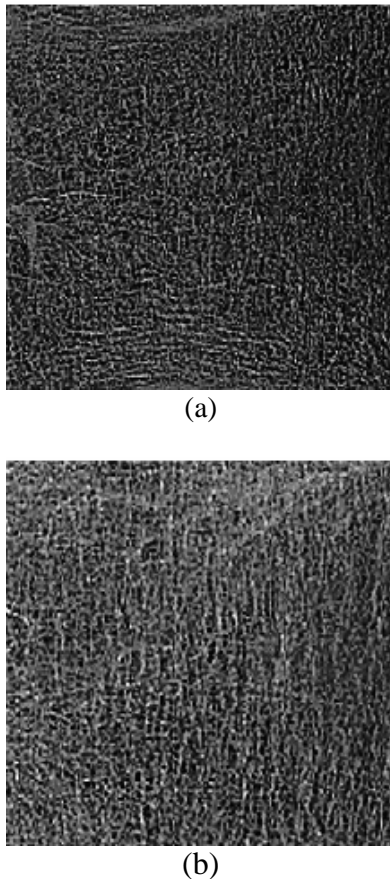| Imaging technique	Texture, structure analysis technique
Conventional radiography	
In vitro: femur-, spine- and calcaneus specimens [42]	Morphological parameters, fractal dimension
	Fast Fourier transform, fractal dimension
In vivo: lumbar spine [37]	Digital skeletons, mathematical filter techniques (« white top
Metacarpals and phalanges [38][39]	hat », Co-occurrence matrices
Distal radius [38]	Morphological parameters, digital skeletons
Calcaneus	Fractal dimension
Magnification radiography	
In vitro: spine specimens [40]	Morphological parameters, fractal dimension, digital skeletons, mathematical filter techniques (« white top hat »), Co-occurrence matrices
In vivo: lumbar spine [40]	Fractal dimension
High-resolution CT	
In vitro: spine, femur and ilium specimens [41]	Fractal dimension, 2D and 3D parameters analogous to histomorphometry
In vivo: lumbar spine and distal radius [43]	Digital skeletons, « Run-length » method, fractal dimension, 2D and 3D parameters analogous to histomorphometry
High-resolution MRI	2D and 3D parameters analogous to histomorphometry, fractal
In vitro: femur and spine specimens [41]	dimension, digital skeletons, autocorrelation
In vivo: distal radius [44] and calcaneus [45]	Morphological parameters, fractal dimension, digital skeletons, autocorrelation, tubularity

(a)

(b)

Fig. 11. Magnification radiographs of two vertebral spine specimens with (a) a high and (b) with a low maximum compressive strength. Note the differences in trabecular structure, with a more vertical orientation of the trabeculae in the weaker specimen, which also appears more coarse.

The Results gives 2.42 for fractal dimension in figure 11 (a), and 2.44 in figure 11 (b), the BMD in this last figure is important, we can see that the fractal dimension gives good result and is correlated to the BMD in this case.

7.2 High-resolution CT

Using HRCT in vivo an in-plane spatial resolution of up to 400 μm and a slice thickness of 1 mm are obtained with clinical scanners; thus, trabecular architecture is subjected to partial volume effects, and individual trabeculae are not depicted. However, the "pseudo-trabecular" structure depicted by images obtained (Fig. 12) correlates with biomechanical measures of bone and the trabecular architecture [41]. Micro-CT systems are under development with spatial resolutions of 28±250 μm. Most of these systems can only be used in vitro for small tissue samples, but some can be

applied to the peripheral skeleton (distal radius) in vivo with a spatial resolution of 170 x 170 x 480 μm [43].

(a)

(b)

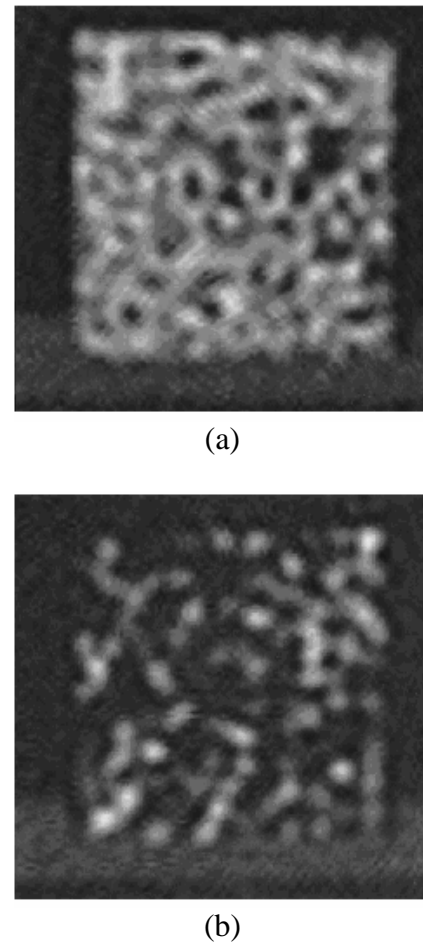**Fig. 12.** High-resolution CT of two bone cube images obtained from the spine (spatial resolution 400 x 400 x 1000 μm) with (a) a dense trabecular structure and a high elastic modulus, and (b) with a scarce trabecular structure and a low elastic modulus, and. Note the « pseudo-trabecular structure » due to partial volume effects.

In this experiment, the results are 1.63 for fractal dimension in figure 12 (a), and 1.85 in the Figure 12 (b), we can notice the degree of BMD is more important in High-resolution CT.

7.3 High-resolution MR imaging

Modern high-field (1.5-T) clinical scanners with fast gradients and optimized coil design provide spatial resolutions of up to 150 μm in plane and slice thicknesses as low as 250 μm; these spatial resolutions have been obtained in vitro in bone

specimens and in vivo in the phalanges, the distal radius and the calcaneus [44]. Using small bore scanners with higher field strengths, even higher spatial resolutions can be obtained up to isotropic voxel sizes of 50 μm [42]. Using HRMRI, however, imaging problems inherent to MRI and technical parameters have to be considered. Due to susceptibility effects between bone and bone marrow, the trabeculae may appear thicker in gradient-echo images compared with spinecho images. In order to obtain images that are comparable, imaging parameters have to be standardized. Since most of the texture parameters require binarized images, a thresholding technique with a high reproducibility has to be used. Intensity-derived thresholding techniques based on the histogram of signal intensities and internal calibration techniques have been used [46].
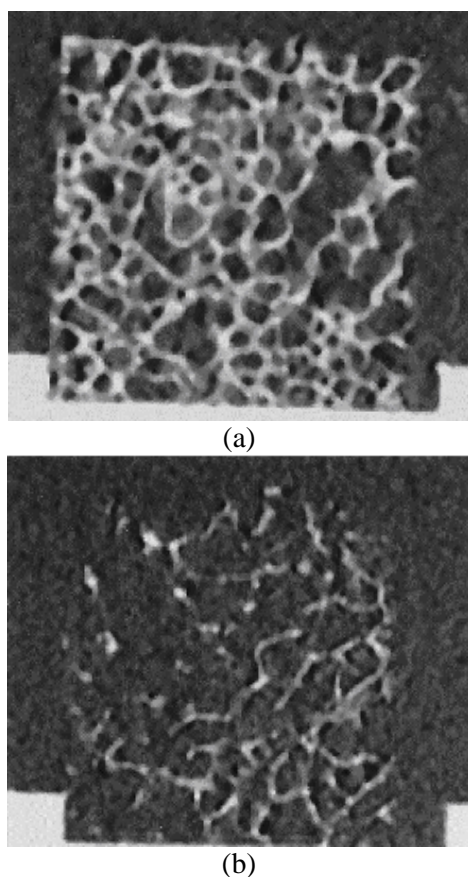

(a)

(b)

Fig. 13. High-resolution MR image obtained from humain cadaver spines (resolution 117 x 156 x 300 μm) with a ascarce trabecular structure and a low elastic modulus, and b with a dense trabecular structure and a high elastic modulus. Compared with the CT image (Fig 12) the trabecular structure is depicted with fewer spatial volume effects and thus reflects the true histomorphological structure better.

It seems quite possible to use the method on MR data, thus avoiding the radiation dose associated with HRCT or DXA, although optimum parameters (e.g. the pulse sequence) have still to be determined. Investigation of the impact of the new structural parameter as a replacement for the morphological analysis is in progress. By combining several parameters, such as BMD in the cortical and the tranecular area, and the fractal classification.

For this last test of images, the results obtained are 1.27 for fractal dimension in figure 13 (a), and 1.80 in figure 13 (b).

The technique of fractal dimension is very powerful and accurate, and this has been demonstrated by comparison with other methods, the difference in healthy bone and osteoporotic bone gives a different fractal dimensions ($D_{osteoporotic}$-$D_{healthy}$). We can conclude that our method has given good results in the detection of osteoporosis in all techniques of imaging.

Future research can be directed to study the evolution of the disease; in this case the osteoporosis can be improved significantly by its medical treatment which can be divided into tree classes:

1- Medication: by prescribing the most common drugs which are bisphosphonates, strontium ranelate and teriparatide.

2- Nutrition: calcium is required to support bone growth, and some studies have shown that a high intake of vitamin D reduces fractures in the elderly.

3- Physical Exercise: multiple studies have shown that aerobics, weight bearing, and resistance exercises can all maintain or increase BMD in postmenopausal women.

Also we can direct the research to predict the osteoporosis and to find the exact degree of the disease with the fractal dimension, in this case one takes several images from a patient's bone according to different age (time) and calculates the fractal dimension; therefore, by using the comparative method of fractal dimension, we can predict the state of the osteoporosis, i.e. we can estimate the time when the disease began, this is one way to monitor the onset of osteoporosis.

Some research can be carried out regarding the risk of bone fracture. There is a correlation between the latter and the BMD; when a risk of bone fracture is presented, we take a radiographic image and calculate its fractal dimension, and this value is taken as a reference to predict the probability of bone fracture.

Also further work is needed to select optimum

texture parameters from a variety of known approaches, including wavelet analysis and mathematical morphology derived features. Also, high-resolution flat bed transparency scanner is being used at present for image digitization with an increased accuracy compared to the CCD camera. First experiments show that fractal dimensions computed for scanned radiographic films demonstrate significantly higher correlation to BMD compared with CCD-recorded images.

8. Conclusion

Throughout this paper we studied the bone mineral density with the fractal dimension in radiographic images of two dimension, after an introduction on the theory of the fractals and its dimension, we have introduced the radiographic images, we discussed that these images was complex and non-linear, for the calculation of their fractal dimension it would have been necessary to find a method that can be freed from the existence of the phenomenon of the statistical random elements that these images present. For that, the box counting method is up to the task and gave good results. We did not only calculate the fractal dimension, we also noticed that the range of the box sizes influenced much of the calculation for this dimension. For that we presented some calculations of fractal dimension corresponding to certain range of r, however, extreme care must be taken in the choice of this range for the analysis. The choice of size for these boxes is worked out for better calculation of the fractal dimension. We have seen the fractal dimension is a very powerful tool for the detection of BMD; we found a new approach that reduces the cost of the estimation of BMD. This method uses a simple X-ray which has been preprocessed to improve the quality; the calculation of the fractal dimension of a subject is achieved compared to a reference fractal dimension of a healthy bone. Finally the method has been tested in other imaging techniques and gave positive results. The importance and usefulness of the fractal concept can be summarized as follows:
1. Fractals possess mathematically strange properties and imply very interesting novel physical phenomena.
2. Fractals are suitable to model complicated real systems.
3. Fractals allow for the application of rigorous scaling and renormalization methods without approximations.

References:

[1] X1. B.B Mandelbrot, *The Fractal Geometry of Nature*. W.H. Freeman and Company, 1983.
[2] X2. K. Falconer, *Fractal Geometry: Mathematical Foundations and Applications*. John Wiley & Sons, 2003.
[3] X3. M .Dalstra, A. Huiskes, EV. Odgaard *Mechanical and textural properties of pelvic trabecular bone*, J Biomech 27, 1993, pp : 375-389.
[4] X4. WHO Scientific Group, *the Prevention and Management of Osteoporosis, (*2000 : Geneva, Switzerland) (2003), Retrieved on 2007-05-31.
[5] X5. T. Mengko, J.T. Pramudito, *Texture Analysis of Proximal Femur Radiographs for Osteoporosis Assessment*, Wseas Transactions on Computers, Issue 1, Volume 3, January 2004, pp : 92 – 97.
[6] X6. N. Furuya, K. Nakamura, I. Kashima, *Morphometric analysis of digital radiographic bone images for trabecular bone structure*, Oral Radiology, Volume 18, Number 2 / decembre 2002, pp : 81 – 93.
[7] X7. H.E. Engan, K.A. Ingebrigtsen, K.G. Oygarden, E.K. Hagen, L. Hoff, *P3F-1 Nonlinear Ultrasound Detection of Osteoporosis*, Norwegian Univ. of Sci. & Technol., Trondheim; april 2007, pp : 2096 – 2099.
[8] X8. A Zaia, R. Eleonori, P. Maponi, R. Rossi, R. Murri, *Medical imaging and Osteoporosis : Fractal's lacunarity analysis of trabecular bone in MR images*, Computer-Based Medical Systems, 2005. 18th IEEE Symposium on computer-based Medical Systems (CBMS'05), June 2005, pp: 3 – 8.
[9] X9. A. Materka, P. Cichy, J. Tuliszkiewicz: *Texture Analysis of X-Ray Images for Detection of Changes in Bone Mass and Structure*, Infotech Oulu Workshop on Texture Analysis in Machine Vision, Oulu, Finland, 1999,pp: 29-34.
[10] X10. N. Phanthuna, F. Cheevasuvit, K. Dejhan, S. Chitwong, *Image Enhancement with Minimum Mean Brightness Error via Automatic Histogram Dividing*, Wseas Transactions on Signal Processing, Issue 2, Volume 3, February 2007, pp : 255 – 261.
[11] X11. M. Stork, D. Mayer, J. Hrusak,*One Dimensional Nonlinear Adaptive Filters for Impulse Noise Suppression*, Wseas Transactions on Signal Processing, Issue 3, Volume 2, march 2006, pp : 337 –342.
[12] X12. Y. Wang, H. Liao, T. Lee, *Applied Variable Step Size Algorithm to Dual-Adaptive Noise Canceller*, Wseas Transactions on Signal

Processing, Issue 10, Volume 3, October 2007, pp : 445 – 452.

[13] X13. M. Hensel, T. Pralow, R. Grigat, *Noise Modeling and a Prefiltering Approach for Real-Time Estimation of Signal-Dependent Quantum Noise*, Wseas Transactions on Signal Processing, Issue 2, Volume 3, February 2007, pp : 171 – 178.

[14] X14. J.F Gouyet, *Physique et structures fractales*, 1992, Masson paris.

[15] X15. H. Maître, *Le traitement des images*, 2003, Lavoisier paris.

[16] X16 I.M. Sokolov, J. Klafter, A. Blumen: Phys. Today 55, 2002, 48.

[17] X17 P. Pfeifer: Chimia 39, 1985, 120.

[18] X18. K. Fouroutan-pour, P. Dutilleul, D.L. Smith, Advances in the implementation of the box-counting methode of fractal dimension estimation, *Applied Mathematics and computation 105*, 1999 pp.195-210, .

[19] X19. R.Voss - Random fractals: charaterization and measurement, in Scaling phenomena and disordred systems, *in R. Pynn & A. Skjeltorp eds, plenum press, New york*, 1986, pp.1-11.

[20] X20. J.M.Keller, S.Chen, R.M.Crownover - Texture description and segmentation through fractal geometry, *CVGIP, 45*, 1989, pp.150-166.

[21] X21. N.Sarkar, B.B.Chaudhuri - An efficient approch to estimate fractal dimension of textural images, *Pattern Recognition, vol. 25, n°9*, 1992, pp.1035-1041.

[22] X22. J.P. Cocquerez, S. Philipp, *Analyse d'images: filtrage et segmentation*, Masson paris, 1995.

[23] X23. B.H. Kaye, *A Random walk thrugh*, Fractal Dimensions, Weinheim, New York, 1994.

[24] X24. J, Soddel, R, Seviour, *Using box counting techniques for measuring shape of colonies of filamentous micro-organisms*, in: R.J. Stonier, X.H. Yu (Eds), Complex Systems: Mechanism of adaptation, IOS Press, Amsterdam, 1994b.

[25] X25. K. Harrar, L. Hamami, *The box counting method for evaluate the fractal dimension in radiographic images*, 6th WSEAS international conference on circuits, systems, electronics, control & signal processing, 2007, pp : 385-390.

[26] X26. K. Imai, M. Ikeda, Y. Enchi, T.Niimi, *Fractal-Feature Distance Analysis of Radiographic Image*, Academic Radiology, Volume 14, Issue 2, 2007, pp.37-143.

[27] X27. RS. Weinstein, S. Majumdar, *Fractal geometry and vertebral compression fractures*, J Bone Miner RES, 1994, pp: 1797 – 1802.

[28] X28. R. Habra, G. Jacquet, R. Jenanne, et al, *Determination of fractal scales on trabecular bone X-ray images*, fractals 1994, pp : 451 – 456.

[29] X29. C. L. Benhamou, R. Harba, E. Lespessailles, et al, *Changes in fractal dimension of trabecular bone in osteoporosis : A preliminary study*. In: Nonnenmacher TF, editor, Fractals in biology and medicine. Basel: Birkhauser-verlag, 1993, pp : 307 – 317.

[30] X30. P. Caliguri, M.L. Giger, M. Favus, *Multifractal radiographic analysis of osteoporosis*, Med Phys, 1994, pp : 503 – 508.

[31] X31. M.A. haidekker, R. Andresen, C. J. G. Evertsz, D. Banzer, H. O. Peitgen, *Assessing the degree of osteoporosis in the axial skeleton using dependence of the fractal dimension on the grey level threshold*, The british journal of radiology, 1997, pp : 586 – 593.

[32] X32. S. Shoupeng, Q. Peiwen, *A Fractal-Dimension-Based Signal-Processing Technique and Its Use for Nondestructive Testing*, Russian Journal of Nondestructive Testing, 2007, pp : 270 – 280.

[33] X33. P. Kotowski, *Fractal dimension of metallic fracture surface*, Springer Science+Business Media, 2006, pp : 269 : 286.

[34] X34. M. Dannowski, A. Block, Fractal geometry and root system structures of heterogeneous plant communities, Plant and Soil, 2005, pp : 61–76.

[35] X35. U. Gonzales-Barron, F. Butler, Fractal texture analysis of bread crumb digital images, Springer-Verlag 2007, pp : 721 : 729.

[36] X36. E. Lespessailles, J. Roux, C. Benhamou, M. Arlot, E. Eynard, R. Harba, C. Padonou, P. Meunier, *Fractal analysis of bone texture on os calcis radiographs compared with trabecular microarchitecture analyzed by histomorphometry*. Calcif Tissue Int, 1998, pp: 121- 125.

[37] X37. P. Caligiuri, M. L. Giger, M. Favus, *Multifractal radiographic analysis of osteoporosis*, Med Phys 21, 1994, pp: 503 - 508

[38] X38. W. Geraets, P. van der Stelt, C. Netelenbos, P. Elders, *A new method for automatic recognition of the radiographic trabecular pattern*. J Bone Mineral Res 5, 1990, pp : 227 – 232.

[39] X39. J.F. Veenland, J.L. Grashuis, E.S. Gelsema, A.L.D. Beckers, C. van Kujik, *Texture analysis of trabecular bone in radiographs to detect Osteoporosis*. Symposium for Computer Assisted Radiology, 1994, pp : 77 – 82.

[40] X40. J.C. Buckland-Wright, J. Lynch, J. Rymer, I. Fogelman, *Fractal signature analysis of macroradiographs measures trabecular*

organization in lumbar vertebrae of postmenopausal women. Calcif Tissue Int 54, 1994, pp: 106 – 112.

[41] X41. T. Link, S. Majumdar, J. Lin, P. Augat, R. Gould, D. Newitt, X. Ouyang, T. Lang, A. Mathur, H. Genant, *Assessment of trabecular structure using high-resolution CT images and texture analysis*. J Comput Assist Tomogr 22, 1998, pp : 15 – 24.

[42] X42. H. Chung, F. Wehrli, J. William, S. Kugelmass, S . *Wehrli, Quantitative analysis of trabecular microstructure by 400 MHz nuclear magnetic resonance imaging*. J Bone Mineral Res 10, 1995, pp : 803 - 811.

[43] X43. R. Mueller, T. Hildebrand, H. Hauselmann, P. Ruegsegger, *In vivo reproducibility of three-dimensional structural properties of noninvasive bone biopsies using 3D-pQCT*. J Bone Mineral Res 11, 1996, pp : 1745 – 1750.

[44] X44. S. Majumdar, H. Genant, S. Grampp, D. Newitt, V. Truong, J. Lin, A. Mathur, *Correlation of trabecular bone structure with age*, bone mineral density and osteoporotic status: in vivo studies in the distal radius using high resolution magnetic resonance imaging. J Bone Mineral Res 12, 1997, pp : 111- 118.

[45] X45. T. Link, S. Majumdar, P. Augat, J. Lin, D. Newitt, Y. Lu, N. Lane, H. Genant, *In vivo high resolution MRI of the calcaneus: differences in trabecular structure in osteoporosis patients*. J Bone Mineral Res 13, 1998, pp : 1175 – 1182.

[46] X46. X. Ouyang, K. Selby, P. Lang, S. Majumdar, H. Genant, *High resolution MR imaging of the calcaneus: age-related changes in trabecular structure and comparison with DXA measurements*. Calcif Tissue Int 60, 1997, pp : 139 – 147.